

Contents lists available at ScienceDirect

Petroleum Science

journal homepage: www.keaipublishing.com/en/journals/petroleum-science



Original Paper

Synergistic catalysis of the N-hydroxyphthalimide on flower-like bimetallic metal-organic frameworks for boosting oxidative desulfurization



Jing He a , Kun Zhu a , Wei Jiang $^{a,\,*}$, Dong-Ao Zhu a , Lin-Hua Zhu b , Hai-Yan Huang a , Wen-Shuai Zhu a , Hua-Ming Li $^{a,\,**}$

ARTICLE INFO

Article history: Received 15 February 2023 Received in revised form 25 April 2023 Accepted 16 August 2023 Available online 18 August 2023

Edited by Jia-Jia Fei and Min Li

Keywords:
Metal-organic frameworks
Doped
Bimetallic
N-hydroxyphthalimide
Aerobic processes
Oxidative desulfurization

ABSTRACT

Synergic catalytic effect between active sites and supports greatly determines the catalytic activity for the aerobic oxidative desulfurization of fuel oils. In this work, Ni-doped Co-based bimetallic metalorganic framework (CoNi-MOF) is fabricated to disperse N-hydroxyphthalimide (NHPI), in which the whole catalyst provides plentiful synergic catalytic effect to improve the performance of oxidative desulfurization (ODS). As a bimetallic MOF, the second metal Ni doping results in the flower-like morphology and the modification of electronic properties, which ensure the exposure of NHPI and strengthen the synergistic effect of the overall catalyst. Compared with the monometallic Co-MOF and naked NHPI, the NHPI@CoNi-MOF triggers the efficient activation of molecular oxygen and improves the ODS performance without an initiator. The sulfur removal of dibenzothiophene-based model oil reaches 96.4% over the NHPI@CoNi-MOF catalyst in 8 h of reaction. Furthermore, the catalytic product of this aerobic ODS reaction is sulfone, which is adsorbed on the catalyst surface due to the difference in polarity. This work provides new insight and strategy for the design of a strong synergic catalytic effect between NHPI and bimetallic supports toward high-activity aerobic ODS materials.

© 2023 The Authors. Publishing services by Elsevier B.V. on behalf of KeAi Communications Co. Ltd. This is an open access article under the CC BY-NC-ND license (http://creativecommons.org/licenses/by-nc-nd/

4.0/).

1. Introduction

Recently, serious environmental pollution, such as haze and acid rain, asks for more imperious demands for clean energy. The toxic SO_x produced by the combustion of sulfides in diesel fuels is a factor causing air pollution (Cheng et al., 2021; Choudhary et al., 2006; Dong et al., 2022; Li et al., 2020, 2022; Liu et al., 2022; Wu et al., 2023). As a result, countries in the world have progressively implemented increasingly stringent regulations to limit sulfur concentrations in diesel fuels to less than 10 ppm (Jiang et al., 2022; Rajendran et al., 2020, 2022; Yang et al., 2019). And the pursuit of clean diesel is an inevitable trend (Zhong et al., 2023). At present, the widely applied hydrodesulfurization technology exhibits high

catalytic activity in the conversion of sulfur compounds. And it failed to remove the aromatic sulfur compounds even at high temperatures because of the steric hindrance of the sulfur atom (Cheng et al., 2021). Hence, a variety of desulfurization technologies emerged. Based on previous research, oxidative desulfurization (ODS) has become an alternative method under mild conditions and has already attracted wide attention (Astle et al., 2019; Bhadra and Jhung, 2021; Jiang et al., 2019; Smolders et al., 2019; Song et al., 2019; Ye et al., 2021; Zou et al., 2021). The research on ODS technology is focused on high-activity catalysts (Dou and Wang, 2019; Jiang et al., 2020; Mao et al., 2023; Wang et al., 2020, 2022; Wu et al., 2023; Ye et al., 2020). Therefore, it is increasingly critical to study and design the high activity catalysts from a principle.

N-hydroxyphthalimide (NHPI), a cheap and nontoxic assistant catalyst, exhibits excellent catalytic performance under mild conditions, which makes it an environmentally friendly organic catalyst with potential applications (Kishioka, 2022; Xu et al., 2022; Yang et al., 2022). The catalytic processes involving NHPI undergo a

^a Institute for Energy Research, Jiangsu University, Zhenjiang, 212013, Jiangsu, China

^b College of Chemistry and Chemical Engineering, Hainan Normal University, Key Laboratory of Water Pollution Treatment and Resource Reuse of Hainan Province, Haikou, 571158, Hainan, China

^{*} Corresponding author.

^{**} Corresponding author. E-mail addresses: jiangwei@ujs.edu.cn (W. Jiang), lhm@ujs.edu.cn (H.-M. Li).

radical pathway, but the catalytic oxidative desulfurization performance of NHPI monomer is still low (Wang et al., 2021). Many carriers were applied to disperse NHPI to obtain high catalytic activity, such as molecular sieves, ultra-thin layered boron nitride and biomass-based porous carbon, etc. (Gao et al., 2022; Lu et al., 2022; Yang et al., 2008). In these studies, the high surface area of the carrier and the synergistic catalysis effect on NHPI were considered and received a great deal of attention. However, homogeneous initiators are usually necessary to assist the proper functioning of the catalyst containing NHPI (Gao et al., 2022; Lu et al., 2022), leading to possible contamination of fuel oil. On the other hand, to catalyze the conversion of organic compounds more efficiently, NHPI in combination with metal sites has already become an efficient method for the activation of molecular oxygen. Hence, the increasing popularity of regulating the catalytic behavior of NHPI catalyst by changing the metallic properties, morphology, and pore environment has stimulated our research interest.

Metal-organic frameworks (MOFs) are a new class of porous material formed by metal clusters and organic ligands. They have drawn extensive attention as a potential material for various applications in adsorption, catalysis, separations, and sensing over the past decades (Cui et al., 2023; Fu et al., 2018; Younas et al., 2020). Especially in the field of catalysis, due to their plentiful porosity, high specific surface area and open metal sites, MOFs containing transition metals not only serve as an appealing platform to confine effective active sites but also play a synergistic catalytic role for the selective conversion of aromatic sulfur compounds (Shen et al., 2021). Recently, studies on dispersing active sites by MOFs have made progress. Pliekhov et al. (2018) designed an impregnation coating strategy to modify N.N'dihydroxypyromellitimide on the surface of Co-based MOFs, leading to a remarkable enhancement in aerobic oxidation of toluene. Also, with the assistance of polyoxometalate, Zhao and Wu (2017) introduced NHPI as a catalyst to provide a useful backup to the biomimetic metalloporphyrin MOFs and form an enzyme-like catalysis system, which showed excellent aerobic oxidation of arylalkanes. However, the study concerned with the synergistic catalysis between metal sites and NHPI is still far from being well discussed, which is important to understand how these systems work.

In this work, nickel atoms were doped in the porous Co-based MOFs (CoNi-MOFs) to regulate the morphology and the composition, with the applied to the dispersion of NHPI. The porous CoNi-MOFs coupled with NHPI catalyst demonstrated remarkable catalytic performance for the ODS of diesel fuels. Furthermore, the physicochemical and electronic proper ties of catalysts were investigated. The possible catalytic mechanism over series catalysts was also analyzed by electron spin resonance spectra and active species quenching experiment.

2. Experimental section

2.1. Synthesis of Co-MOF, Ni-MOF, CoNi-MOF and NHPI@CoNi-MOF

To synthesize Co-MOF, 0.4 mmol of cobalt acetate tetrahydrate and 1,4-dicarboxybenzene were dissolved into 50 mL of the mixture, which was composed of the acetonitrile and N,N'-dimethylformamide at a 3:2 vol ratio. Then, the metal salt solution was dropped into the solution and aged at room temperature for 24 h. The precipitates were centrifugated and dried in a vacuum oven at 80 °C. The crude products were washed with CH_2Cl_2 in a Soxhlet extractor to remove the remnant. The final powder obtained after drying was named as Co-MOF. At the same time, the Ni-MOF was prepared with a similar method, just replacing the cobalt acetate tetrahydrate with an equal molar of nickel acetate.

To synthesize CoNi-MOF, the whole procedure is similar to the above process (Yang et al., 2014), in which the composition of the

metal source is a 0.4 mmol mixture of cobalt acetate tetrahydrate and nickel acetate with different molar ratios of Co to Ni (8:2, 7:3, 6:4, 5:5). The resulting samples were named as Co₈Ni₂-MOF, Co₇Ni₃-MOF, Co₆Ni₄-MOF, Co₅Ni₅-MOF accordingly.

To synthesize NHPI@CoNi-MOF, 0.075 g of CoNi-MOF powder and 0.025 g of NHPI were dispersed in absolute ethanol in 50 mL of the vessel. Then the dispersion was ultrasonic for 30 min and dried in a rotary evaporator. The obtained powder was named as NHPI@CoNi-MOF.

2.2. Catalytic reaction procedure

The model diesel fuel with a sulfur content of 200 ppm was obtained via dissolving dibenzothiophene (DBT), 4-methyldibenzothiophene (4-MDBT), and 4,6-dimethyldibenzothiophene (4,6-DMDBT) in dodecane with hexadecane as the internal standard (He et al., 2021). The catalytic ODS experiments were carried out in a reactor setup at $110-130~^{\circ}\text{C}$. A certain number of catalysts, model diesel fuels and a constant flow of oxygen were added to the reactor. After a certain reaction time, the represented sulfur content was analyzed through gas chromatography. The sulfur removal was calculated by the formula as follows:

Sulfur removal (%) =
$$\frac{(C_0 - C_t)}{C_0} * 100\%$$
 (1)

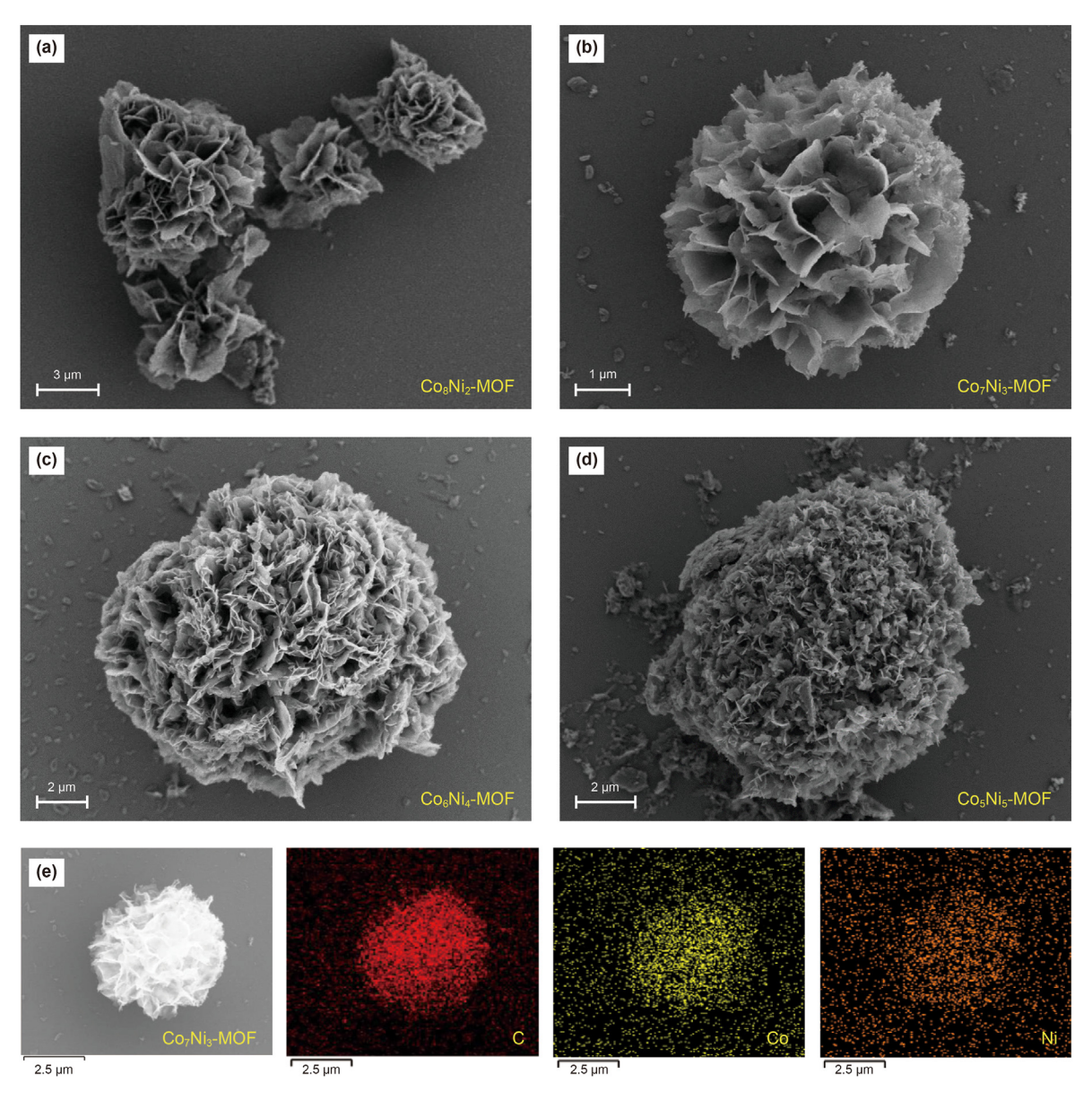
During the free radical quenching experiment, 20 mmol of free radical quenchers are added into the reaction system to quench the possible active radical species. The products after the ODS reaction were analyzed by gas chromatography-mass spectrometry (GC-MS, Agilent 7890-5975C). The method of GC-MS is similar to the previously reported (He et al., 2019). The detailed experiment is described below. After the reaction, the used catalysts were separated and washed with 1 mL of carbon tetrachloride. The washing layer and the model fuel oils after the ODS reaction were filtered and analyzed by GC-MS. The vaporizing chamber of the injection port was set to 250 °C. The split mode is adopted throughout the analysis. The split ratio was set at 50:1. The carrier gas uses highpurity helium with a purity of 99.999%. The auxiliary temperature, ion source temperature, and quadrupole temperature of MS were set at 280, 230 and 150 °C. The oven temperature was programmed to heat samples for analysis and identification.

The recycling experiment was carried out as follows: after a typical catalytic ODS experiment, the reaction solution was fully standing at room temperature, until the model fuel oils and catalysts were fully separated. The upper model fuel oils were taken out as far as possible through the dropper, and then the remaining catalyst was dried in the oven at 80 °C for 12 h. The used catalyst and fresh model fuel oils were added into the reaction bottle and the desulfurization experiment steps were repeated until the catalytic performance decreased significantly.

3. Results and discussion

3.1. Characterization of the catalyst

To observe the microtopography of the sample, SEM images are shown in Fig. 1 and Fig. S1. A significant number of flakes can be observed for the sample Co-MOF, while the Ni-MOF also presents a flaky appearance (Fig. S1). By adjusting the proportion of metal source Co/Ni, the morphology of CoNi-MOF began to change. The flakes of Co-MOF gather together and gradually assemble into a 3D porous structure with the addition of Ni²⁺ ions (Fig. 1(a)). Immediately, the 3D flower-like CoNi-MOF particles are formed when the



 $\textbf{Fig. 1.} \ \ \text{The SEM image of (a)} \ \ Co_{8}Ni_{2}-\text{MOF}; \ \textbf{(b)} \ \ Co_{7}Ni_{3}-\text{MOF}; \ \textbf{(c)} \ \ Co_{6}Ni_{4}-\text{MOF}; \ \textbf{(d)} \ \ Co_{5}Ni_{5}-\text{MOF}; \ \textbf{(e)} \ \ \text{element mapping of } Co_{7}Ni_{3}-\text{MOF}; \ \textbf{(d)} \ \ \text{Co}_{5}Ni_{5}-\text{MOF}; \ \textbf{(e)} \ \ \text{element mapping of } Co_{7}Ni_{3}-\text{MOF}; \ \textbf{(e)} \ \ \text{element mapping of } Co_{7}Ni_{3}-\text{MOF}; \ \textbf{(e)} \ \ \text{element mapping } Co_{7}Ni_{3}-\text{MOF}; \ \textbf{(e)} \ \ \text{element mapping } Co_{7}Ni_{3}-\text{MOF}; \ \textbf{(e)} \ \ \text{element } Co_{7}Ni_{7}-\text{MOF}; \ \textbf{(e)} \ \ \text{element } Co_{7}Ni_{7}-\text{MOF}$

Co/Ni ratio is 7:3 (Fig. 1(b)). The 3D flower-like structure, accompanied by abundant stacked cavities and pore channels, is very helpful in anchoring active components. As the further increasing of Ni²⁺ ions content, the intercalation of flower-like MOF is becoming tight, resulting in a compact flower structure (Fig. 1(c)). When the precursor contains an equal mole of Co²⁺ and Ni²⁺ ions, the structure of flower-like microspheres can still be maintained, but the pores and cavities are almost completely blocked, forming a tight spherical structure (Fig. 1(d)). The results show that largescale 3D flower-like CoNi-MOF can be synthesized by adding the Ni precursor solution with a heating mixing method. The content of metal precursor has remarkable effects on the morphology of MOF, which is similar to the previous report (Yang et al., 2014). Besides, the element mapping and EDS results also reflect that the Ni component has already been incorporated in the Co-MOF (Fig. 1(e)). As shown in Figs. S2 and S3, the C, O, Co and Ni are evenly distributed in other samples, in which the intensity of the mapping corresponds to the content of the element. Also, Table S1 shows that the actual doping amount of metal agrees well with the

theoretical doping value, which indicates the successful doping of metal Ni^{2+} to a certain extent.

The crystal structure of porous MOFs was investigated by XRD pattern. As shown in Fig. 2, doped Co-MOF, especially Co₇Ni₃-MOF, with the most stereoscopic flower morphology and excellent crystallinity is selected as the support. NHPI with catalytic oxidation performance serves as the active site. Fig. 2(a) shows the XRD patterns of NHPI, Co₇Ni₃-MOF and NHPI@Co₇Ni₃-MOF, respectively. The diffraction peaks at 8.9° , 15.7° , 17.5° , 25.3° and 28.0° are assigned to the characteristic peak of Co₇Ni₃-MOF. And NHPI shows sharp diffraction peaks at 7.9°, 11.1°, 11.8°, 15.2°, 15.9°, and 23.9°, which matches with standard card (PDF#34-1725). For hybrid NHPI@Co7Ni3-MOF, all the well-resolved diffraction peaks of Co₇Ni₃-MOF and NHPI are observed, indicating that the active site NHPI is successfully immobilized without damaging the crystalline structure of the Co₇Ni₃-MOF support. The FT-IR spectra of NHPI, Co₇Ni₃-MOF and NHPI@Co₇Ni₃-MOF were analyzed. As shown in Fig. 2(b), the characteristic peaks at 3602 and 3429 cm⁻¹ belong to the stretching and bending vibration of the dissociative hydroxyl

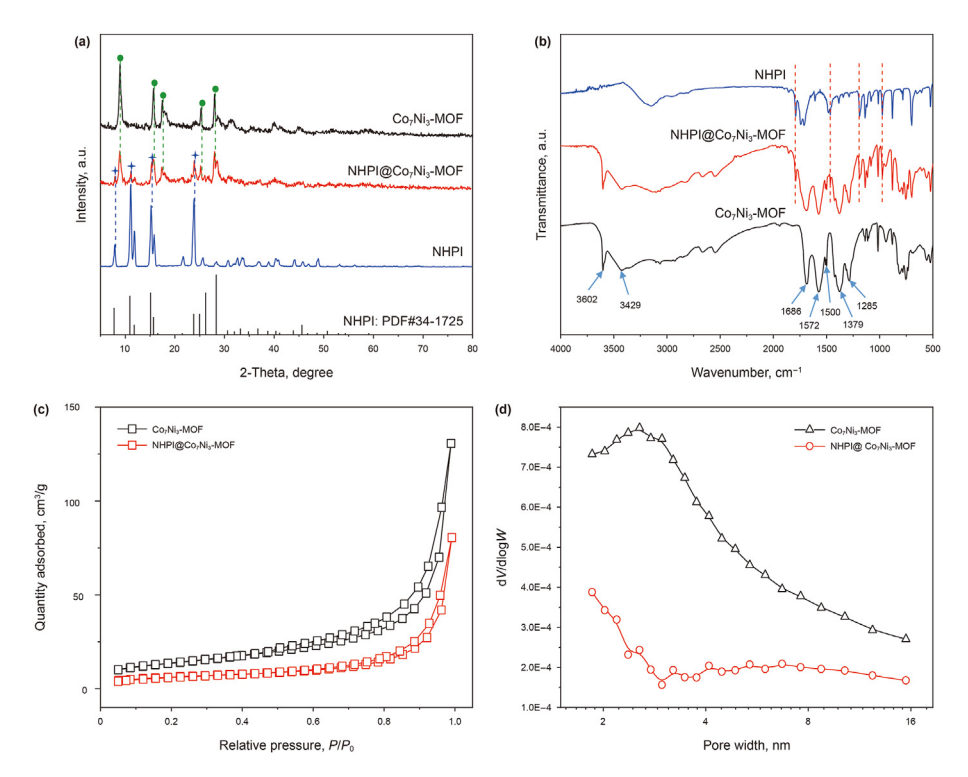


Fig. 2. (a) XRD patterns; (b) The FTIR spectra; (c) The nitrogen adsorption-desorption isotherms; (d) The pore size distribution.

group in coordinated water molecules, respectively. The peaks at 1572 and 1500 cm $^{-1}$ correspond to the stretching vibration of C=C from organic ligand terephthalic acid (Soni et al., 2009). The stretching vibration of C=O from the carboxyl group on the ligand shows a peak at 1686 cm⁻¹ (Agustin and Tamura, 2021), while the stretching vibration of C-N in the residual solvent molecule is shown at 1285 cm⁻¹. Besides, the symmetric stretching vibration of C=O, C=N and benzene ring C-H out-of-plane vibration belonging to NHPI at 1790, 1186 and 978 cm⁻¹ is observed. The nitrogen adsorption-desorption isotherms were carried out to evaluate the pore characteristics of different porous MOFs. Fig. 2(c) shows the isothermal curve and pore size distribution diagram of Co₇Ni₃-MOF and NHPI@Co7Ni3-MOF. The isotherm curves of different MOFs are ascribed to type IV according to the international union of pure and applied chemistry (IUPAC) classification, which belongs to mesoporous materials. The specific surface area of porous MOFs increases as the construction of flower-like MOFs, where the specific surface area of Co₇Ni₃-MOF rises to 48.4 m²/g (Fig. 2(c), black line). As the intercalation is denser, the flower morphology collapses gradually. A significant decrease in specific surface area and pore volume can be observed after NHPI is incorporated (Fig. 2(c), red line). As shown by SEM in Fig. S4, the NHPI occupied the pore channel of MOF during the impregnation process. Therefore, the densest pore size range (2-3 nm) also shifts to ~2 nm (Fig. 2(d)).

To identify the chemical states of each element in porous MOF, the XPS measurements were carried out. As shown in Fig. 3, C, O, Co, and Ni are observed on the surface of Co₇Ni₃-MOF, indicating the incorporation of Ni. The pollution carbon signal of all samples is calibrated to 284.8 eV. The additional peak and shoulder peak at 288.5 and 286.2 eV were assigned to the carbonyl groups (C=O) and C=N species, respectively (Lu et al., 2018). The main Co 2p peak consists of 6 sub-peaks in 3 groups. The blue and green peaks are the different oxidation states of Co in the Co₇Ni₃-MOF, while the red peaks are satellite peaks. After Ni²⁺ incorporation, the binding

energy of Co 2p_{3/2} upshifts significantly from 780.8 to 781.2 eV, indicating that the introduction of Ni is likely to change the chemical environment of Co and make it in the electron-deficient state. Similarly, the main peak of Ni 2p was also fitted, which is composed of 4 sub-peaks. The peaks located at 855.9 and 873.6 eV are ascribed to the binding energy of Ni 2p_{3/2} and Ni 2p_{1/2}, which are not significantly changed after Ni²⁺ incorporation. This may be related to the same chemical environments around Ni in the Ni-MOFs and Co₇Ni₃-MOF. For NHPl@Co₇Ni₃-MOF samples (Fig. S5), there is no significant difference in the chemical environment of each element in the catalyst whether NHPl is supported or not, except for the special NHPl group, which indicated that the structure of the support was not damaged.

3.2. Evaluation of catalytic performance

The ODS behaviors of flower-like porous Co₇Ni₃-MOF, NHPI, and NHPI@CoNi-MOF materials are evaluated by a three-phase system with O₂ as an oxidant. As shown in Fig. 4(a), the NHPI@CoNi-MOF composite catalyst displays significantly enhanced ODS performance than a single component catalyst. In particular, 96.4% of sulfur removal can be achieved by NHPI@Co₇Ni₃-MOF, while the desulfurization performance over NHPI and Co₇Ni₃-MOF catalyst is only 33.2% and 18.0% after 8 h of reaction. This result confirms that the loading strategy is beneficial to the improvement of ODS performance. The effect on catalytic ODS performance of various MOFs, with different compositions and structures, is shown in Fig. 4(b). NHPI@Ni-MOF exhibits extremely poor desulfurization performance with a sulfur removal of 7.8% while NHPI@Co-MOF displays a higher sulfur removal of 73.2%, indicating that Co-MOF is more likely to act as a co-catalyst.

To further regulate the structure and properties of Co-based MOF, bimetallic MOF was obtained via a doping strategy. The second metal nickel doping changes the morphology and structure of Co-based MOF, resulting in a 3D flower-like CoNi-MOF. The flower-

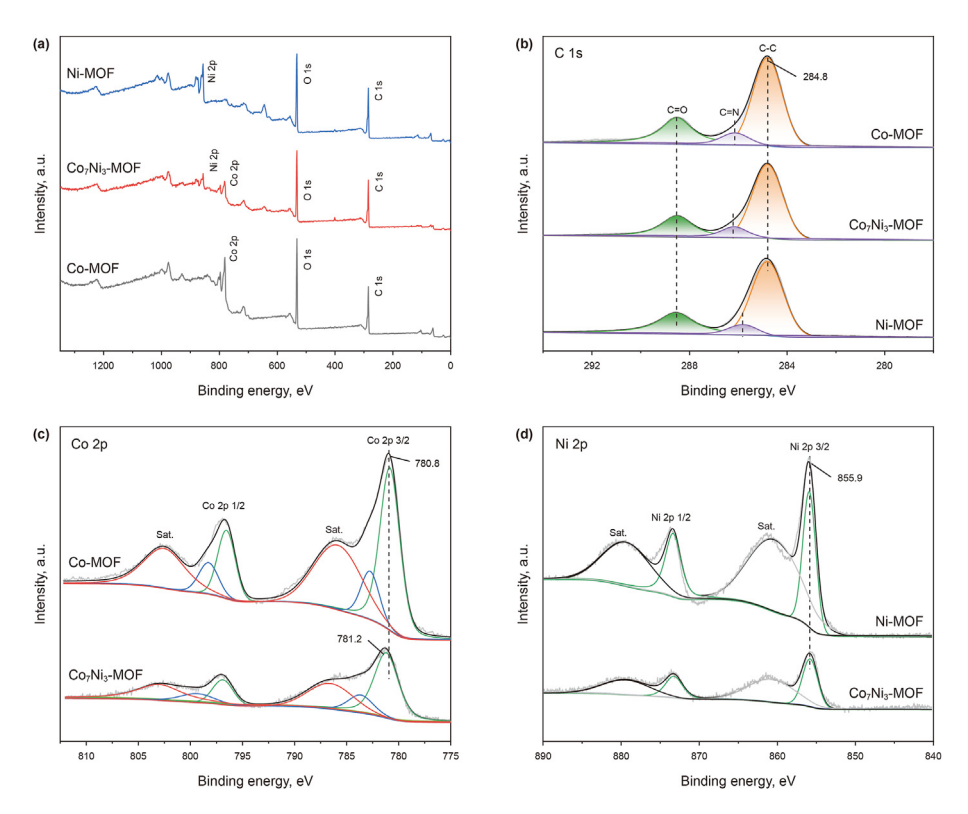


Fig. 3. (a) XPS of survey spectra, (b) C1s, (c) Co 2p, and (d) Ni 2p for the Co-MOF, Ni-MOF, and Co₇Ni₃-MOF composites, respectively.

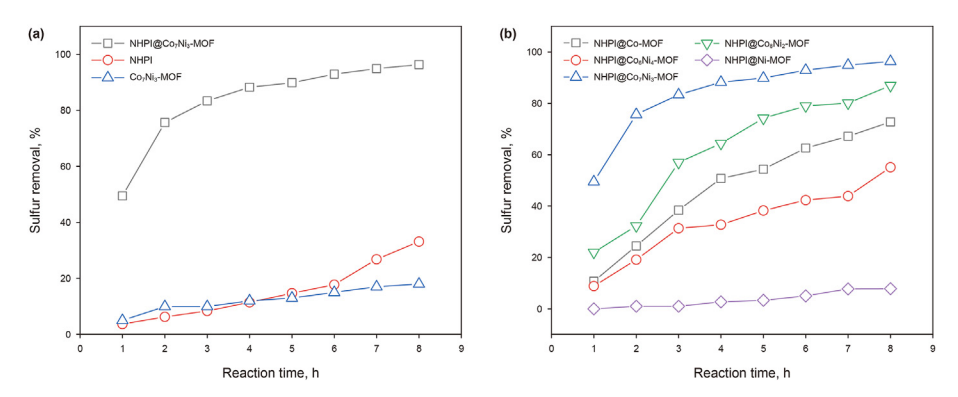


Fig. 4. (a) The comparison of the desulfurization performance of Co_7Ni_3 -MOF, NHPI, and NHPI@ Co_7Ni_3 -MOF; (b) The desulfurization performance of catalysts with different ratios of Co and Ni. Reaction condition: $T = 120 \, ^{\circ}C$, m (catalysts) = 0.05 g, V (model diesel fuels) = 20 mL, V (O_2) = 200 cm³/min.

like structure possesses abundant stacked cavities and pore channels, which is helpful in anchoring active components NHPI. When those CoNi-MOFs containing different Co/Ni ratios were used to support the active component NHPI, the catalytic performance of the catalyst was also significantly different. After 8 h of reaction, the sulfur removal of NHPI@Co₈Ni₂-MOF, NHPI@Co₇Ni₃-MOF, and NHPI@Co₆Ni₄-MOF was 86.9%, 96.4%, and 55.1%, respectively. Only in the appropriate ratio (Co₇Ni₃-MOF), the obtained catalyst (NHPI@Co₇Ni₃-MOF) shows the capability of deep desulfurization. In other cases, the main reason for the failure of deep desulfurization is that the active component Co and its suitable chemical environment in the bimetallic MOF jointly determine the catalytic ODS performance of the overall catalyst. Therefore, it is considered that the morphology, elemental composition, and chemical environment of the bimetallic MOF significantly affect the catalytic activity of the NHPI@CoNi-MOF catalyst. As we know, NHPI shows

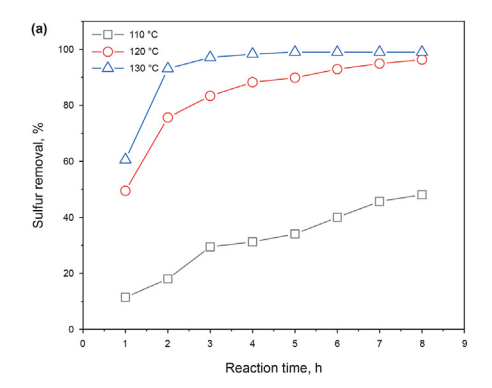
catalytic activity for the oxidation of organic sulfide, but the condition of this reaction is rather harsh. As shown in Table S2, ionic liquids and isobutyraldehyde (BuCHO) are used to assist the oxidation of sulfides. It has also been observed that the amount of BuCHO is critical to the conversion efficiency of sulfide. To further expose NHPI active centers, NHPI has also been dispersed on the surface of two-dimensional boron nitride and porous carbon to achieve deep oxidative desulfurization. However, due to the lack of the co-catalytic effect of Co-based MOF, the boron nitride or porous carbon dispersed NHPI catalysts cannot completely remove aromatic sulfur in diesel fuels. The initiators including azodiisobutyronitrile and cobalt acetate are essential for the above catalysts to achieve ultra-deep desulfurization. For such NHPI/h-BN-30 and NHPI/PC catalysts, the desulfurization efficiency will be severely inhibited if the initiator is absent. However, extractants and initiators are not necessary for this work. Ultra-deep desulfurization

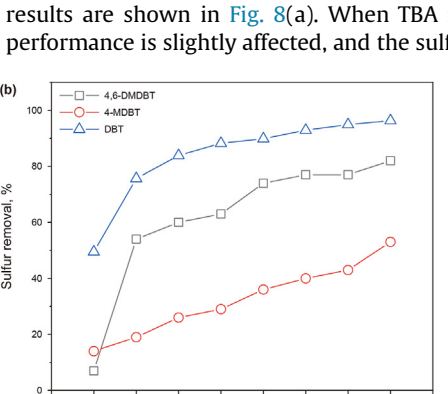
can be achieved under mild conditions due to the abundant hierarchical structure and the synergic catalysis effect. Thus, compared with the previously reported catalysts, the NHPI@CoNi-MOF catalyst shows better catalytic activity without an initiator.

3.3. Optimization of ODS reaction

The catalytic performance of NHPI@Co7Ni3-MOF was tested at different temperatures. The results are shown in Fig. 5. Only 48.1% of organic aromatic sulfur is removed after 8 h of reaction at 110 °C. As the reaction temperature increased to 120 °C, the catalytic ODS performance reaches 96.4% after 8 h. When the reaction is conducted at 130 °C for 2 h, desulfurization performance can reach more than 90.0%. Furthermore, the $\ln (C_t/C_0)$ vs reaction time is plotted to investigate the reaction kinetics. As shown in Fig. S6, the fitting results show a linear correlation between $\ln (C_t/C_0)$ and t, suggesting that this catalytic ODS belongs to a pseudo-first-order reaction (He et al., 2015). From the point of view of reaction kinetics, as the temperature of the reaction increases, the rate constant k is also increasing. According to the Arrhenius equation (Jia et al., 2019; Liu et al., 2023), the ln k vs temperature is plotted in Fig. S7 to investigate the activation energies (E_a). With the addition of NHPI@Co7Ni3-MOF catalyst, the Ea of DBT oxidation over NHPI@Co₇Ni₃-MOF catalyst is 19.7 kJ/mol. The content of NHPI also affects the desulfurization performance of catalytic oxidation (Fig. S8). When Co₇Ni₃-MOF was used as a suitable carrier and NHPI was loaded at 25 wt%, the desulfurization efficiency was better.

Different sulfur-containing substrates are employed to study the desulfurization efficiency. As shown in Fig. 5(b), under the same ODS conditions, the catalytic removals of DBT, 4-MDBT, and 4,6-DMDBT are 96.4%, 53.0%, and 82.0%, respectively. Such differences in desulfurization performance may be closely related to the molecular structure of sulfur-containing substrates. According to the literature (Li et al., 2016), the electron density on sulfur atoms and steric hindrance of the branched chain are the two most critical factors for the oxidation of aromatic sulfur. The electron density of sulfur atoms of DBT, 4-MDBT, and 4,6-DMDBT is 5.758, 5.739, and 5.760 (Otsuki et al., 2000). In terms of electron density, the reactivity sequence of a series of aromatic organic sulfides is as follows: DBT < 4-MDBT < 4,6-DMDBT, indicating that DBT should be most difficult to be oxidized. However, unlike the 4-MDBT and 4,6 DMDBT, the molecular structure of DBT does not contain any branched chains, meaning that there is no steric hindrance near the sulfur atoms. The steric hindrance of methyl groups in 4-MDBT and 4,6 DMDBT will result in limited contact between active sites and sulfur atoms. Thus, the final reaction activity order of these aromatic organic sulfur is as follows: DBT > 4,6-DMDBT > 4-MDBT, which is consistent with the experimental results.





Reaction time, h

Fig. 5. (a) Desulfurization performance of catalysts at different temperatures; (b) Effect of different substrates on sulfur removal. Reaction condition: T = 120 °C, m (catalysts) = 0.05 g, V (model diesel fuels) = 20 mL, V (V02) = 200 cm³/min.

3.4. Investigate catalyst stability

The stability and recyclability of the NHPI@Co₇Ni₃-MOF catalyst were also investigated by multiple ODS experiments. Typically, after running a desulfurization reaction, the sulfur-free fuel oils are separated and the fresh fuels are added into the reactor for the next run. As shown in Fig. 6(a), the sulfur removal remains at about 95% within 4 cycles. In the subsequent cycles, the catalytic activity gradually decreases and the sulfur removal of the fifth and sixth runs are 87.1% and 67.4% respectively. The FT-IR spectrum for the reused NHPI@Co7Ni3-MOF after the cycles is carried out and shown in Fig. 6(b). The reused NHPI@Co7Ni3-MOF is regenerated by washing with CCl₄. Results show that the structure of Co₇Ni₃-MOF is retained without damage, but the overall structure of the NHPI@Co₇Ni₃-MOF catalyst has changed a lot. The characteristic peaks attributed to NHPI were weakened, indicating that the NHPI component in the NHPI@Co7Ni3-MOF catalyst was lost after recycling, which may be the main reason for the substantial reduction of catalyst performance after six recycles.

3.5. Analysis of the products

The reaction products and their distribution were analyzed by GC-MS of the reaction solution. Generally, after the ODS reaction, the catalyst is completely separated from the model diesel fuels and extracted by CCl_4 (He et al., 2022). As shown in Fig. 7, a characteristic peak appears at about 7 min of retention time, which belongs to DBT (m/z 184). During the reaction, it can be observed that the characteristic peak of DBT is weakened during the reaction and completely disappeared after the reaction. Finally, the mass spectrum analysis of the CCl_4 extraction solution shows that the molecular ion peak at 216.0 is corresponding to DBTO₂ in Fig. 7 (Jiang et al., 2021). Therefore, DBTO₂ is confirmed as the main oxidation product (Sun et al., 2019; Xing et al., 2022; Xun et al., 2023).

3.6. Identification of active species

To further investigate the reaction mechanism, the radical quenching experiment was carried out. Usually, superoxide radicals and hydroxyl radicals are considered as two main active radicals for the catalytic oxidation of aromatic sulfur compounds (Chu et al., 2023; Jin et al., 2022; Xiong et al., 2022). Herein, benzoquinone (BQ) and *tert*-butanol (TBA) are used as radical quenchers of superoxide radical and hydroxyl radical, respectively. During the ODS process, an appropriate amount of free radical quenchers agents is added to quench possible active radical species. The experimental results are shown in Fig. 8(a). When TBA is added, the catalytic performance is slightly affected, and the sulfur removal can still be

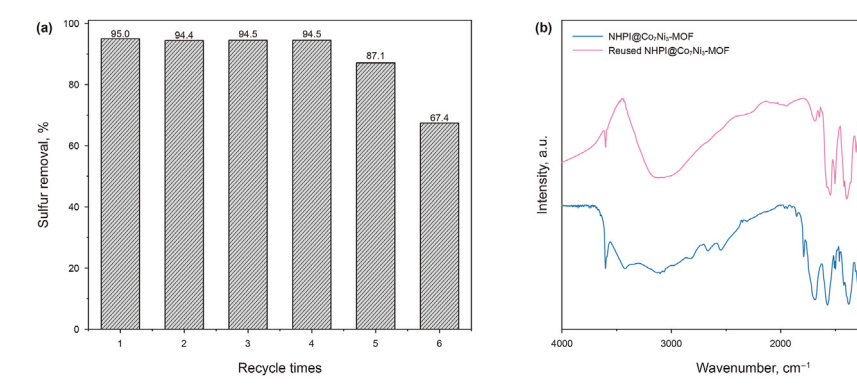


Fig. 6. (a) Recycling performance of NHPI@Co₇Ni₃-MOF on sulfur removal; (b) FTIR spectra of the prepared catalysts. Reaction condition: $T = 120 \, ^{\circ}\text{C}$, $v \, (O_2) = 200 \, \text{cm}^3/\text{min}$, $m \, (\text{catalysts}) = 0.05 \, \text{g}$, $V \, (\text{model diesel fuels}) = 20 \, \text{mL}$.

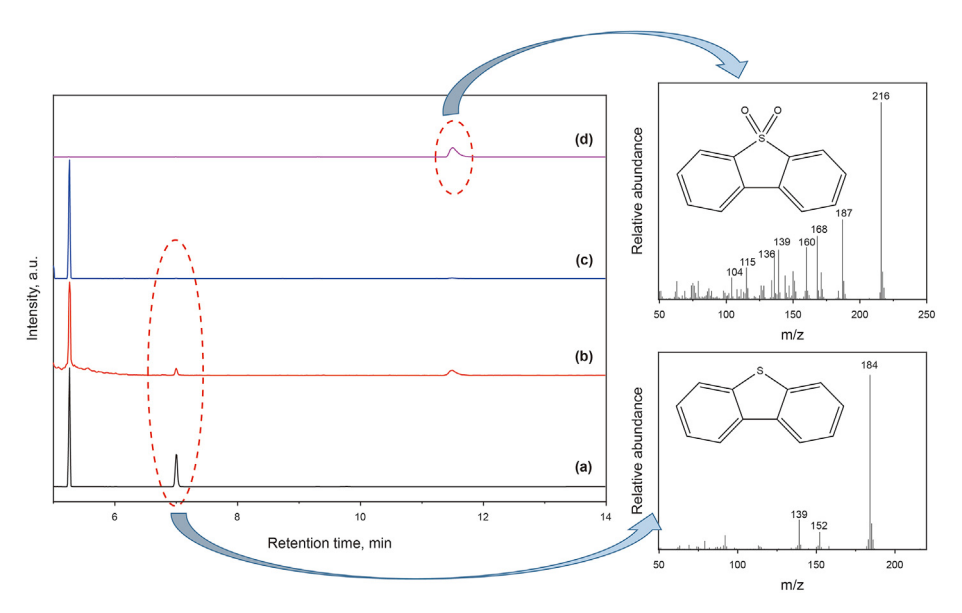


Fig. 7. GC-MS analysis of each stage of the reaction process. (a) the model diesel fuels before reaction; (b) the model diesel fuels during reaction; (c) the model diesel fuels after reaction; (d) the extractant phase of the catalyst after reaction.

maintained at 85.4%. While the sulfur removal decreases to 31.2% after the addition of BQ. The above results show that the main active radical species might be superoxide radicals $(O_2^{\bullet-})$, and there is also a small amount of hydroxyl radical (\bullet OH). Furthermore, the active species is tested by the ESR spectra with 5,5'-dimethyl-1-

pirroline-N-oxide (DMPO) as the spin trap. As shown in Fig. 8(b), there is no free radical signal that appears when the 3D flower-like Co_7Ni_3 -MOF and NHPI are used as the catalyst, respectively. When NHPI@Co_7Ni_3-MOF is added into the reaction system, a strong sextet peak signal appears in the ESR pattern, indicating that

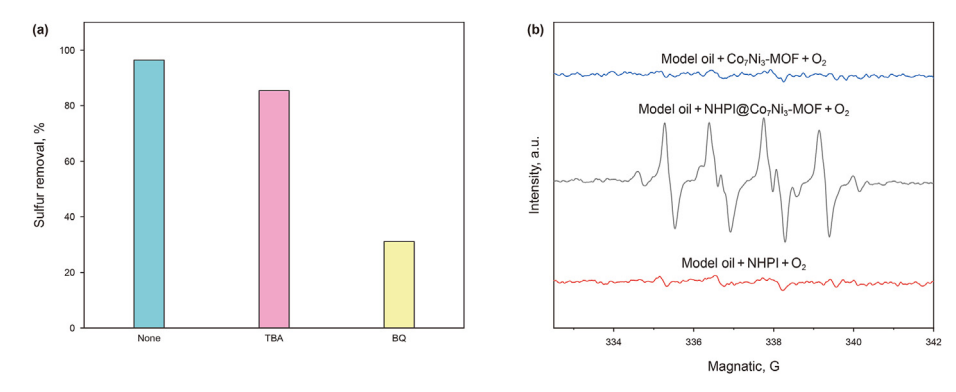


Fig. 8. (a) Investigation of selective quenching experiments; (b) ESR analysis of free radicals generated during the reaction. Reaction condition: T = 120 °C, m (catalysts) = 0.05 g, V (model diesel fuels) = 20 mL, V (O₂) = 200 cm³/min.

molecular oxygen can be activated to form a superoxide radical. Furthermore, the NHPl@Co $_7$ Ni $_3$ -MOF catalyst with synergistic catalytic properties promotes the formation of superoxide radicals, which play a key role in the catalytic ODS.

4. Conclusion

To sum up, towards clean diesel fuels, the homogeneous NHPI catalyst was anchored on the Ni-doped Co-based MOFs for aerobic oxidative desulfurization. The morphology of Co-based MOF and the chemical environment of Co were adjusted by nickel doping, resulting in the modification of the electronic structure of the active metal site. The synergistic catalytic activities of NHPI are greatly enhanced by the bimetallic-compatible porous flower-like support. Compared with the monometallic MOF and naked NHPI, the ODS performance of NHPI@Co7Ni3-MOF was greatly improved. The sulfur removal of dibenzothiophene-based model diesel can reach 96.4% without an additional extractant or initiator, which is a significant improvement over the previous work. Also, the catalytic desulfurization process follows the free radical mechanism, in which the superoxide radical plays a key role. The distribution analysis of the products indicated that sulfones were the main products and could be adsorbed by catalysts to obtain clean diesel fuels. Moreover, the NHPI@Co7Ni3-MOF hybrid catalyst can be recycled four times and still reach 95% of ODS activity. The innovation of this paper is that bimetallic flower-like CoNi-MOF with co-catalytic effect is obtained by using cobalt salt as the component of the carrier MOF and further achieves deep desulfurization of diesel oil with synergistic effect between NHPI and bimetallic MOF.

Declaration of competing interest

The authors declare that they have no known competing financial interests or personal relationships that could have appeared to influence the work reported in this paper.

Acknowledgement

This work was financially supported by the National Natural Science Foundation of China (Nos. 21978119, 22202088), Key Research and Development Plan of Hainan Province (ZDYF2022SHFZ285), and Jiangsu Funding Program for Excellent Postdoctoral Talent (2022ZB636)

Appendix A. Supplementary data

Supplementary data to this article can be found online at https://doi.org/10.1016/j.petsci.2023.08.018.

References

- Agustin, A.R., Tamura, K., 2021. Surface modification of TiO₂ nanoparticles with terephthalic acid in supercritical carbon dioxide. J. Supercrit. Fluids. 174, 105245. https://doi.org/10.1016/j.supflu.2021.105245.
- Astle, M.A., Rance, G.A., Loughlin, H.J., et al., 2019. Molybdenum dioxide in carbon nanoreactors as a catalytic nanosponge for the efficient desulfurization of liquid fuels. Adv. Funct. Mater. 29 (17), 1808092. https://doi.org/10.1002/adfm.201808092
- Bhadra, B.N., Jhung, S.H., 2021. Oxidative desulfurization of liquid fuel with tungsten-nitride@porous carbon, derived from MAF-6(Zn) loaded with phosphotungstic acid and melamine. Chem. Eng. J. 419, 129485. https://doi.org/10.1016/j.cej.2021.129485.
- Cheng, H., Cui, Y., Ge, Z., et al., 2021. Insight into the mechanism of tuned extractive desulfurization by aqueous tetrabutylphosphonium bromide. Sep. Purif. Technol. 262, 118342. https://doi.org/10.1016/j.seppur.2021.118342.
- Choudhary, T.V., Malandra, J., Green, J., et al., 2006. Towards clean fuels: molecular-level sulfur reactivity in heavy oils. Angew. Chem. Int. Ed. 45 (20), 3299–3303. https://doi.org/10.1002/anie.200503660.
- Chu, L., Guo, J., Huang, Z., et al., 2023. Excellent catalytic performance over acid-

treated MOF-808(Ce) for oxidative desulfurization of dibenzothiophene. Fuel 332, 126012. https://doi.org/10.1016/j.fuel.2022.126012.

- Cui, H.Y., Zhang, Y.X., Cao, C.S., et al., 2023. Engineering noble-metal-free metal—organic framework composite catalyst for efficient CO₂ conversion under ambient conditions. Chem. Eng. J. 451, 138764. https://doi.org/10.1016/ i.ei.2022.138764.
- Dong, L., Dai, X., Peng, C., et al., 2022. Ultra-deep catalytic adsorptive desulfurization of diesel fuel using Ti-silica gel adsorbent at low Ti-loading. AIChE J. 68 (2), e17493. https://doi.org/10.1002/aic.17493.
- Dou, S.Y., Wang, R., 2019. The C-Si Janus nanoparticles with supported phosphotungstic active component for Pickering emulsion desulfurization of fuel oil without stirring. Chem. Eng. J. 369, 64–76. https://doi.org/10.1016/j.cej.2019.03.050.
- Fu, G.X., Bueken, B., De Vos, D., 2018. MOF catalysts: Zr-metal-organic framework catalysts for oxidative desulfurization and their improvement by postsynthetic ligand exchange. Small Methods 2 (12), 1800059. https://doi.org/10.1002/ smtd 201870059
- Gao, X., Jiang, W., An, X., et al., 2022. Aerobic ultra-deep desulfurization of diesel oil triggered by porous carbon supported organic molecular N-hydroxyphthalimide catalyst. Colloids Surf. A. 641, 128455. https://doi.org/10.1016/ i.colsurfa.2022.128455.
- He, J., Liu, H., Xu, B., et al., 2015. Highly flexible Sub-1 nm tungsten oxide nanobelts as efficient desulfurization catalysts. Small 11 (9–10), 1144–1149. https:// doi.org/10.1002/smll.201401273.
- He, J., Wu, P.W., Lu, L.J., et al., 2019. Synthesis of N,O-doped porous graphene from petroleum coke for deep oxidative desulfurization of fuel. Energy Fuel. 33 (9), 8302–8311. https://doi.org/10.1021/acs.energyfuels.9b01832.
- He, J., Wu, P.W., Chen, L.L., et al., 2021. Dynamically-generated TiO₂ active site on MXene Ti₃C₂: boosting reactive desulfurization. Chem. Eng. J. 416, 129022. https://doi.org/10.1016/j.cej.2021.129022.
- He, J., Zhou, S., Wu, P., et al., 2022. Multi-walled carbon nanotubes coated on defective tungsten oxide for deep oxidative desulfurization of diesel fuels. Fuel Process. Technol. 236, 107399. https://doi.org/10.1016/j.fuproc.2022.107399.
- Jia, Q., He, J., Wu, P., et al., 2019. Tuning interfacial electronic properties of carbon nitride as an efficient catalyst for ultra-deep oxidative desulfurization of fuels. Mol. Catal. 468, 100—108. https://doi.org/10.1016/j.mcat.2019.02.011.
- Jiang, W., Jia, H., Li, H., et al., 2019. Boric acid-based ternary deep eutectic solvent for extraction and oxidative desulfurization of diesel fuel. Green Chem. 21 (11), 3074–3080. https://doi.org/10.1039/C9GC01004A.
- Jiang, W., Zhu, K., Li, H., et al., 2020. Synergistic effect of dual Brønsted acidic deep eutectic solvents for oxidative desulfurization of diesel fuel. Chem. Eng. J. 394, 124831. https://doi.org/10.1016/j.cej.2020.124831.
- Jiang, W., Xiao, J., Gao, X., et al., 2021. In situ fabrication of hollow silica confined defective molybdenum oxide for enhanced catalytic oxidative desulfurization of diesel fuels. Fuel 305, 121470. https://doi.org/10.1016/j.fuel.2021.121470.
- Jiang, W., An, X., Xiao, J., et al., 2022. Enhanced oxygen activation achieved by robust single chromium atom-derived catalysts in aerobic oxidative desulfurization. ACS Catal. 12 (14), 8623—8631. https://doi.org/10.1021/acscatal.2c01329.
- Jin, D., Yu, G., Li, X., et al., 2022. One-pot extractive and oxidative desulfurization of fuel with ternary dual-acid deep eutectic solvent. Fuel 329, 125513. https:// doi.org/10.1016/j.fuel.2022.125513.
- Kishioka, S., 2022. Electrode reaction of N-hydroxyphthalimide in sulfuric acidacetonitrile mixed solution as a catalytic mediator for alcohol oxidation. Electroanal. Chem. 911, 116166. https://doi.org/10.1016/ji.jelechem.2022.116166.
- Li, A., Song, H.Y., Meng, H., et al., 2022. Steric effects of alkyl dibenzothiophenes: the root cause of frustrating efficacy of heterogeneous desulfurization for real diesel. AIChE J. 68 (5), e17614. https://doi.org/10.1002/aic.17614.
- Li, H.P., Zhu, W.S., Zhu, S.W., et al., 2010. The selectivity for sulfur removal from oils: an insight from conceptual density functional theory. AIChE J. 62 (6), 2087–2100. https://doi.org/10.1002/aic.15161.
- Li, Y.X., Shen, J.X., Peng, S.S., et al., 2020. Enhancing oxidation resistance of Cu(I) by tailoring microenvironment in zeolites for efficient adsorptive desulfurization. Nat. Commun. 11 (1), 3206. https://doi.org/10.1038/s41467-020-17042-6.
- Liu, J.X., Zhang, L., Zhu, J.Y., et al., 2023. Size-dependent surface electronic structure of V₂O₅/TiO₂ for ultra-deep aerobic oxidative desulfurization of diesel. Chem. Eng. Sci. 275 (5), 118749. https://doi.org/10.1016/j.ces.2023.118749.
- Liu, J.X., Liu, X.Q., Yan, R.X., et al., 2022. Active phase morphology engineering of NiMo/Al₂O₃ through La introduction for boosting hydrodesulfurization of 4,6-DMDBT. Petrol. Sci. 20 (2), 1231–1237. https://doi.org/10.1016/j.petsci.2022.09.023.
- Lu, L.J., He, J., Wu, P.W., et al., 2018. Taming electronic properties of boron nitride nanosheets as metal-free catalysts for aerobic oxidative desulfurization of fuels. Green Chem. 20 (19), 4453–4460. https://doi.org/10.1039/C8GC01625A.
- Lu, L.J., Wu, P.W., He, J., et al., 2022. N-hydroxyphthalimide anchored on hexagonal boron nitride as a metal-free heterogeneous catalyst for deep oxidative desulfurization. Petrol. Sci. 19 (3), 1382–1389. https://doi.org/10.1016/ j.petsci.2021.11.010.
- Mao, S.X., Zhou, Q.H., Guo, H.L., et al., 2023. Porous phosphomolybdate-based poly(ionic liquid) hybrids with reversible water absorption for enhancement of oxidative desulfurization. Fuel 333, 126392. https://doi.org/10.1016/ i.fuel.2022.126392.
- Otsuki, S., Nonaka, T., Takashima, N., et al., 2000. Oxidative desulfurization of light gas oil and vacuum gas oil by oxidation and solvent extraction. Energy Fuel. 14 (6), 1232–1239. https://doi.org/10.1021/ef000096i.
- Pliekhov, O., Pliekhova, O., Lavrenčič Štangar, U., et al., 2018. The Co-MOF-74

modified with N,N'-Dihydroxypyromellitimide for selective, solvent free aerobic oxidation of toluene. Catal. Commun. 110, 88–92. https://doi.org/10.1016/i.catcom 2018 03 021

- Rajendran, A., Cui, T.Y., Fan, H.X., et al., 2020. A comprehensive review on oxidative desulfurization catalysts targeting clean energy and environment. J. Mater. Chem. A 8 (5), 2246–2285. https://doi.org/10.1039/C9TA12555H.
- Rajendran, A., Fan, H.X., Cui, T.Y., et al., 2022. Octamolybdates containing MoV and MoVI sites supported on mesoporous tin oxide for oxidative desulfurization of liquid fuels. J. Clean. Prod. 334, 130199. https://doi.org/10.1016/j.jclepro.2021.130199.
- Shen, Y., Pan, T., Wang, L., et al., 2021. Programmable logic in metal—organic frameworks for catalysis. Adv. Mater. 33 (46), 2007442. https://doi.org/10.1002/adma.202007442.
- Smolders, S., Willhammar, T., Krajnc, A., et al., 2019. A titanium(IV)-based metalorganic framework featuring defect-rich Ti-O sheets as an oxidative desulfurization catalyst. Angew. Chem. Int. Ed. 58 (27), 9160–9165. https://doi.org/ 10.1002/anie.201904347.
- Song, J., Li, Y., Cao, P., et al., 2019. Synergic catalysts of polyoxometalate@cationic porous aromatic frameworks: reciprocal modulation of both capture and conversion materials. Adv. Mater. 31 (40), 1902444. https://doi.org/10.1002/ adma.201902444
- Soni, R.K., Soam, S., Dutt, K., 2009. Studies on biodegradability of copolymers of lactic acid, terephthalic acid and ethylene glycol. Polym. Degrad. Stabil. 94 (3), 432–437. https://doi.org/10.1016/j.polymdegradstab.2008.11.014.
- Sun, L., Su, T., Xu, J., et al., 2019. Aerobic oxidative desulfurization coupling of Co polyanion catalysts and p-TsOH-based deep eutectic solvents through a biomimetic approach. Green Chem. 21 (10), 2629–2634. https://doi.org/10.1039/ C8GC03941K
- Wang, H., Shan, S., Li, P., et al., 2022. Deep oxidative desulfurization of model fuel catalyzed by phosphotungstic acid/mesoporous zeolite. React. Kinet. Mech. Catal. 135 (4), 1999–2012. https://doi.org/10.1007/s11144-022-02237-3.
- Wang, L., Zhang, Y., Yao, J., et al., 2021. Metal-free synthesis of sulfones and sulf-oxides through aldehyde-promoted aerobic oxidation of sulfides. Catal. Lett. 152 (4), 1131–1139. https://doi.org/10.1007/s10562-021-03706-5.
- Wang, P.Y., Jiang, L.C., Zou, X.Q., et al., 2020. Confining polyoxometalate clusters into porous aromatic framework materials for catalytic desulfurization of dibenzothiophene. ACS Appl. Mater. Interfaces 12 (23), 25910–25919. https://doi.org/ 10.1021/acsami.0c05392.
- Wu, C., Sun, Z., Ye, C., et al., 2023. Encapsulation of HPW and preparation of composites rich in Zr-defects by manual grinding: synergistic catalysis for efficient oxidative desulfurization at room temperature. Chem. Eng. J. 451, 138906. https://doi.org/10.1016/j.cej.2022.138906.
- Xing, X.X., Guo, H.L., He, T.M., et al., 2022. Tungstovanadate-based ionic liquid catalyst [C₂(MIM)₂]₂VW₁₂O₄₀ used in deep desulfurization for ultraclean fuel with simultaneous recovery of the sulfone product. ACS Sustainable Chem. Eng. 10 (35), 11533—11543. https://doi.org/10.1021/acssuschemeng.2c02973.
- Xiong, J., Li, J., Chen, C., et al., 2022. Universal strategy engineering grain boundaries for catalytic oxidative desulfurization. Appl. Catal. B Environ. 317, 121714.

- https://doi.org/10.1016/j.apcatb.2022.121714.
- Xu, L., Yi, Y., Hu, S., et al., 2022. Unraveling two pathways for NHPI-mediated electrocatalytic oxidation reaction. Electrochim. Acta 403, 139533. https:// doi.org/10.1016/j.electacta.2021.139533.
- Xun, S.H., Le, R.M., Hu, C.C., et al., 2023. Ionic liquid promotes high dispersion of V₂O₅ on 3D porous g-C₃N₄ Carrier to enhance catalytic oxidative desulfurization performance. Energy Fuel. 37, 6276–6280. https://doi.org/10.1021/acs.energyfuels.3c003036276.
- Yang, D., Liu, M., Zhao, W., et al., 2008. A comparative oxidation of cyclohexane catalyzed by N-hydroxyphthalimide and ZSM-5 supported Co(II), Mn(II), Ni(II), Zn(II), Fe(III) with molecular oxygen in the absence of solvents and reductants. Catal. Commun. 9 (14), 2407–2410. https://doi.org/10.1016/j.catcom.2008.05.039.
- Yang, H., Zhang, Q., Zhang, J., et al., 2019. Cellulose nanocrystal shelled with poly(ionic liquid)/polyoxometalate hybrid as efficient catalyst for aerobic oxidative desulfurization. J. Colloid Interface Sci. 554, 572–579. https://doi.org/10.1016/j.icis.2019.07.036.
- Yang, J., Zheng, C., Xiong, P., et al., 2014. Zn-doped Ni-MOF material with a high supercapacitive performance. J. Mater. Chem. A 2 (44), 19005—19010. https:// doi.org/10.1039/c4ta04346d.
- Yang, Y., Ma, J., Wu, J., et al., 2022. Experimental and theoretical study on N-hydroxyphthalimide and its derivatives catalyzed aerobic oxidation of cyclohexylbenzene. Chin. J. Chem. Eng. 44, 124–130. https://doi.org/10.1016/j.ciche.2021.06.017.
- Ye, G., Gu, Y.L., Zhou, W., et al., 2020. Synthesis of defect-rich titanium terephthalate with the assistance of acetic acid for room-temperature oxidative desulfurization of fuel oil. ACS Catal. 10 (3), 2384–2394. https://doi.org/10.1021/ acscatal.9h04937
- Ye, G., Wang, H.L., Chen, W.X., et al., 2021. In situ implanting of single tungsten sites into defective UiO-66(Zr) by solvent-free route for efficient oxidative desulfurization at room temperature. Angew. Chem., Int. Ed. 60 (37), 20318–20324. https://doi.org/10.1002/anie.202107018.
- Younas, M., Rezakazemi, M., Daud, M., et al., 2020. Recent progress and remaining challenges in post-combustion CO₂ capture using metal-organic frameworks (MOFs). Prog. Energ. Combust. 80, 100849. https://doi.org/10.1016/j.pecs.2020.100849.
- Zhao, M., Wu, C.D., 2017. Biomimetic activation of molecular oxygen with a combined metalloporphyrinic framework and co-catalyst platform. ChemCatChem 9 (7), 1192–1196. https://doi.org/10.1002/cctc.201601606.
- Zhong, H., Wei, Z., Man, Y., et al., 2023. Prediction of instantaneous yield of bio-oil in fluidized biomass pyrolysis using long short-term memory network based on computational fluid dynamics data. J. Clean. Prod. 391, 136192. https://doi.org/ 10.1016/j.jclepro.2023.136192.
- Zou, J.C., Lin, Y., Wu, S.H., et al., 2021. Molybdenum dioxide nanoparticles anchored on nitrogen-doped carbon nanotubes as oxidative desulfurization catalysts: role of electron transfer in activity and reusability. Adv. Funct. Mater. 31 (22), 2100442. https://doi.org/10.1002/adfm.202100442.